ScieRxiv

NOT PEER-REVIEWED

Research Article

Magnetic COF-supported single-atom Pt for enhanced anti-markovnikov alkene hydrosilylation

Lingyu Sun[1,2,3], Guodong Cheng[1,2,4], Qihui Dang[1,2,3], Zunfu Hu[1,2], Zhichao Dai[1,2], Zibao Gan[1,2], Yunqiang Sun[1,2*], Xiuwen Zheng[1,3*]

[1]Key Laboratory of Advanced Biomaterials and Nanomedicine in Universities of Shandong, Linyi University, Linyi 276000, Shandong, China.

[2]College of Chemistry and Chemical Engineering, Linyi University, Linyi 276000, Shandong, China.

[3]Qilu Normal University, Jinan 250200, Shandong, China.

[4]State Key Laboratory of Advanced Separation Membrane Materials, School of Material Science and Engineering, Tiangong University, Tianjin 300387, China.

Correspondence to: Prof. Xiuwen Zheng, Prof. Yunqiang Sun, Key Laboratory of Advanced Biomaterials and Nanomedicine in Universities of Shandong, Linyi University, Linyi 276000, Shandong, China. E-mail: zhengxiuwen@lyu.edu.cn; sunyunqiang@lyu.edu.cn

Received: 25 May 2026 | Approved: 02 June 2026 | Online: 02 June 2026

Abstract

The catalytic hydrosilylation of alkenes holds significant value for applications in fine chemical synthesis. However, conventional homogeneous platinum-based catalysts exhibit limitations including low selectivity, residual contamination and metal leaching. Herein, a single-atom platinum catalyst anchored on a magnetic covalent organic framework (Pt-SAC/COF@Fe_3O_4) was fabricated without requiring high-temperature

calcination. Comprehensive characterization (high-angle annular dark-field scanning transmission electron microscopy, X-ray absorption spectroscopy) confirmed that atomically dispersed Pt single atoms anchored on the COF@Fe_3O_4 support. Under mild reaction conditions (80 °C, 10 h), the as-prepared catalyst afforded an alkene yield of 93% with excellent anti-Markovnikov selectivity up to 98%. Notably, the catalytic yield was enhanced by 31% relative to the commercial Pt/C catalyst, demonstrating superior catalytic performance. Owing to the robust anchoring effect of the COF@Fe_3O_4 matrix on atomically dispersed Pt sites and its inherent magnetic properties, the catalyst could be efficiently recovered via magnetic separation for reuse. Remarkably, it retained high stability and efficiency over five catalytic cycles. This work not only demonstrates the precise design of a magnetically responsive catalyst with atomically active centers but also provides a novel strategy for advancing the industrial implementation of anti-Markovnikov alkene hydrosilylation reactions.

Keywords: Heterogeneous catalysis, single-atom catalysts, covalent organic frameworks, magnetic recovery, anti-markovnikov alkene hydrosilylation

INTRODUCTION

Organosilicon materials have recently expanded from traditional applications such as electrical insulation and construction into emerging fields including energy storage, biomedical devices, and advanced coatings[1–5]. This trend necessitates the development of efficient and versatile synthetic routes for organosilicon compounds. Since the seminal work of Speier[6] and Karstedt[7], hydrosilylation has become a key strategy for constructing structurally complex silanes, typically using platinum-based catalysts[8–10]. However, the scarcity and high cost of platinum severely limit its large-scale industrial application. Although cheaper transition metals (e.g., Fe[11], Co[12], Ni[13]) have been explored as alternatives, they face challenges such as difficult catalyst recycling in homogeneous systems and low atomic efficiency in heterogeneous ones. Thus, there is an urgent need for catalytic systems that integrate the advantages of both homogeneous

and heterogeneous catalysis to maximize noble metal utilization.

Single-atom catalysts (SACs), featuring atomically dispersed metal species with nearly complete atomic utilization, bridge the gap between homogeneous and heterogeneous catalysis[14]. Due to their uniform active sites and precisely controlled coordination environment, SACs offer superior catalytic performance with reduced metal consumption. Nevertheless, SACs are prone to aggregation during preparation and catalytic processes. Suitable supports (e.g., zeolites[15], metal-organic frameworks (MOFs)[16] and covalent organic frameworks (COFs)[17]) can confine metal atoms in isolated configurations. Zhao group[18] achieved the Pt single atom catalysts by strategically incorporating triazine, secondary amine, and b-ketoenamine linkages into the COF architecture, transitioning from nanoparticles to single atoms. Hence, the choice of support is critical for SAC stability and activity.

COFs have emerged as excellent catalyst supports owing to their well-defined crystalline structures, tunable pores, and high chemical stability[19–21]. Typically constructed via strong covalent bonds (e.g., imine linkages), the metal-free organic backbone of COFs avoids interference from support-derived metal impurities, COFs exhibit high surface areas and thermal stability[22,23]. Unlike MOFs or metal-containing supports, the organic backbone of COFs avoids interference from support-derived metal impurities, enabling unambiguous characterization of catalytic active sites. For instance, Qian group[24] showed that bimetallic sites in COFs significantly enhance activity and stability in electrocatalytic CO_2 reduction. Despite these merits, the powder form of COFs often hinders solid-liquid separation. To solve this issue, magnetic COF composites (e.g., COF@Fe_3O_4[25]) have been developed, enabling efficient catalyst recovery via magnetic separation.

Magnetic nanoparticles have attracted extensive attention in the field of catalyst immobilization due to their inherent magnetic properties and high stability[26,27]. The porous structure and surface functional groups of COF@Fe_3O_4 composites not only

improve magnetic recoverability but also provide a platform for highly dispersed active sites. Various magnetically recyclable catalysts have been reported, including porous magnetic COF[28], Fe_3O_4-CuO NCs[29] and starch-coated magnetic nanoparticles for palladium catalysis[30]. However, the integration of atomically dispersed SACs with magnetically separable nanoparticles remains largely unexplored. Therefore, developing magnetically supported Pt SACs with well-defined active centers is of practical importance for efficient anti-Markovnikov alkene hydrosilylation.

In this work, we report a magnetically COF@Fe_3O_4 supported platinum single-atom catalyst (Pt-SAC/COF@Fe_3O_4), synthesized under mild conditions (125 °C, Scheme 1). This approach avoids the high-temperature calcination that often causes agglomeration of SACs and overcomes the trade-off among activity, stability, and recyclability. Experimental results demonstrate that the synthesized Pt-SAC/COF@Fe_3O_4 achieves 93% alkene yield with 98% anti-Markovnikov selectivity in hydrosilylation reactions, retains 99% selectivity after five cycles, and shows negligible Pt leaching. Moreover, it can be magnetically separated from the reaction mixture within 2 min. This work provides a generalizable strategy for designing magnetically recoverable, atomically precise catalysts.

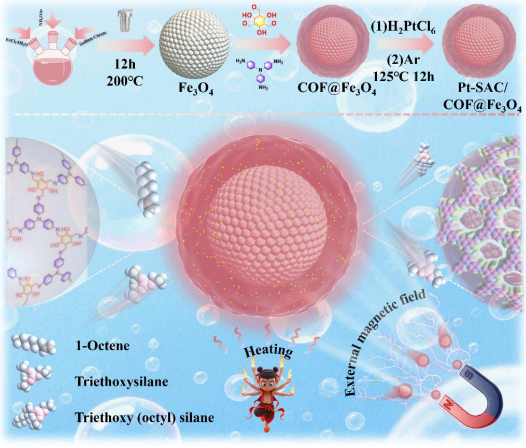

Scheme 1. The fabrication of Pt-SAC/@COF@Fe_3O_4 catalyst and Pt-SAC/@COF@Fe_3O_4 catalyze anti-Markovnikov alkene hydrosilylation reaction.

MATERIALS AND METHODS

Materials

Iron chloride hexahydrate ($FeCl_3 \cdot 6H_2O$, AR) was purchased from Shanghai Macklin Biochemical Technology Co., Ltd. Ammonium acetate (NH_4OAc, AR) was purchased from Foshan Xilong Chemical Co., Ltd. Citric acid trisodium salt (AR), 1,3,5-trimethylbenzene (AR), dodecane (GR), tetrahydrofuran (THF, AR), toluene (AR) and p-xylene (AR) were purchased from Shanghai Lin'en Technology Development Co., Ltd. 4,4',4''-Triaminotriphenylamine (Pa, AR) and 2,4,6-trihydroxybenzene-1,3,5-tricarbaldehyde (Tp, AR) were purchased from Shanghai Bide Pharmaceutical Technology Co., Ltd. Acetonitrile (ACN, AR), ethyl acetate (EA, AR), methanol (AR) and ethanol (AR) were purchased from Tianjin Yongda Chemical Reagent Co., Ltd. All silicanes (AR) and alkenes (AR) were obtained from Shanghai Lin'en Technology Development Co., Ltd.

Preparation of Fe_3O_4

The Fe_3O_4 nanomaterials were prepared through a modified reported method[31]. Typically, ethylene glycol (50 mL) in a three-necked flask was used to dissolve $FeCl_3 \cdot 6H_2O$ (1.35 g), NH_4OAc (3.85 g), and sodium citrate (0.4 g) under continuous ultrasonication. Next, the mixture was vigorously stirred at 160 °C for 1 h to afford a black homogeneous solution and then transferred into a Teflon-lined stainless-steel autoclave (100 mL capacity). The mixture was heated at 200 °C for 12 h. The product was washed with aqueous and ethanol several times in sequence when it was cooled to room temperature naturally and then was dried at 60 °C.

Preparation of COF@Fe_3O_4

The synthesis of COF@Fe_3O_4 was referred to relevant studies[32] Typically, Fe_3O_4 (46.4 mg, 0.2 mmol) was thoroughly dispersed in 10 mL of a mesitylene/THF mixed solvent (2:1, v/v) inside a 50 mL round-bottom flask via ultrasonication. Subsequently, Tp (49.6 mg, 0.228 mmol) and Pa (96.1 mg, 0.338 mmol) were sequentially introduced

into the suspension. The resulting mixture was transferred and sealed in a 50 mL Teflon-lined stainless-steel autoclave, followed by solvothermal treatment at 100 °C for 72 h. After naturally cooling to room temperature, the precipitate was purified by soaking and washing with a mixed solvent of MeOH/$CHCl_3$ for 6 h. Finally, drying the product at 60 °C yielded the COF@Fe_3O_4 composite as a brown powder.

Preparation of Pt-SAC/COF@Fe_3O_4 catalyst

Typically, 50 mg of COF@Fe_3O_4 was dispersed in 30 mL of acetonitrile inside a 50 mL round-bottom flask under gentle stirring, followed by the slow dropwise addition of an H_2PtCl_6 acetonitrile solution (100 μL, 10 mg/mL). The reaction proceeded at room temperature for 24 h. The product was collected by centrifugal separation, purified by washing several times with anhydrous acetonitrile to remove residual precursors, and dried under vacuum at 60 °C overnight to obtain Pt NPs/COF@Fe_3O_4. This intermediate was subsequently transferred to a tube furnace and calcined at 125 °C for 1 h under an Ar purge, employing a heating rate of 5 °C/min to successfully yield the Pt-SAC/COF@Fe_3O_4 catalyst. The mass fraction of Pt in the final product was determined to be 0.75 wt.% via ICP-OES measurement.

Representative experimental procedure for catalytic anti-Markovnikov hydrosilylation of alkenes

First, silicane (1.7 mmol), alkene (1 mmol), and Pt-SAC/COF@Fe_3O_4 catalyst (10 mg) were added to a 15 mL side-armed Schlenk tube containing 1 mL of p-xylene. The reaction system was placed in an oil bath maintained at 80 °C with continuous stirring. Upon completion of the reaction, the catalyst was magnetically separated from the mixture using an external magnet. The resulting solution was subsequently filtered through a membrane filter. Finally, the yield and selectivity of reaction was determined by gas-chromatography (GC) using dodecane as the internal standard.

Characterization and analytical evaluation

The structural and chemical attributes of the catalyst were interrogated using a suite of characterization techniques: Transmission electron microscope (TEM) and high resolution transmission electron microscopy (HR-TEM) images were determined on a JEOL-2100 transmission electron microscope. The structure and morphology of the prepared samples were examined using a sub-angstrom resolution aberration-corrected high-angle annular dark-field scanning transmission electron microscopy (AC HAADF-STEM) on a Titan cubed G260-300 with an accelerating voltage of 200 kV, equipped with two Cs-correctors (probe and image Cs-correctors). AC HAADF-STEM coupled with energy dispersive X-ray spectroscopy mapping (EDS-Mapping) was conducted on a JEOL ARM-200F field emission transmission electron microscope. X-ray diffraction (XRD) patterns were obtained from a Smart Lab X-ray diffractometer (RIGAKU) using Cu Kα radiation (λ = 0.15418 nm). The metal content in the catalyst was measured by inductively coupled plasma-optical emission spectrometry (ICP-OES). X-ray photoelectron spectroscopy (XPS) was conducted on a Thermo ScientificTM K-AlphaTM+ spectrometer equipped with a monochromatic Al Kα X-ray source (1,486.6 eV) operating at 100 W. Samples were analyzed under vacuum ($P < 10^{-8}$ mbar) with a pass energy of 150 eV (survey scans) or 50 eV (high-resolution scans). All peaks would be calibrated with C1s peak binding energy at 284.8 eV for adventitious carbon. The X-ray absorption fine structures (XAFS) were conducted using the 8 C nanoprobe XAFS beamline (BL8C) of Pohang light source (PLS-II) in the 3.0 GeV storage ring, with a ring current of 250 mA. The X-ray beam was monochromated by a Si (111) double crystal where the beam intensity was reduced by 30% to eliminate the higher-order harmonics. The X-ray beam was then delivered to a secondary source aperture where the beam size was adjusted to be 0.5 mm (v) × 1 mm (h). The XAFS spectra were collected in both transmission and fluorescence modes. The obtained spectra were processed using a Demeter software. For wavelet transform (WT) analysis, the χ(k) exported from Athena was imported into the Hama Fortran code. The UV-vis spectra were carried out on a NANO DROP 2000 spectrophotometer, respectively. GC analysis was conducted on a Thermo Trace 1,300 series GC with an FID detector using

a capillary column (TR-5MS, from Thermo Scientific, length 30 m, i.d. 0.25 mm, film 0.25 μm).

RESULTS AND DISCUSSION

Synthesis and characterization of the Pt-SAC/COF@Fe_3O_4

The synthetic procedure of Pt-SAC/COF@Fe_3O_4 is illustrated in Scheme 1. First, according to the previous report[31] with a slight modification, the magnetic core of Fe_3O_4 nanoparticles was successfully synthesized.

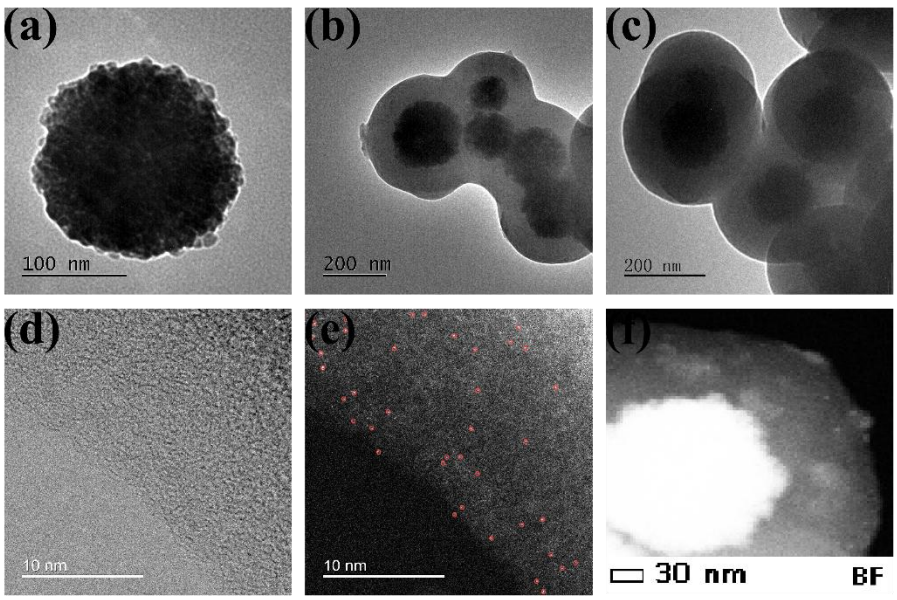

Figure 1. (a-c) TEM image of Fe_3O_4, COF@ Fe_3O_4, Pt-SAC/COF@Fe_3O_4; (d) HR-TEM image of Pt-SAC/COF@Fe_3O_4; (e) AC HAADF-STEM image of Pt-SAC/COF@Fe_3O_4; (f) HAADF-STEM image of Pt-SAC/COF@Fe_3O_4.

TEM image [Figure 1a] exhibited that Fe_3O_4 nanoparticles with a roughly spherical morphology and sizes on the order of approximately 197 nm. Subsequently, COF@Fe_3O_4 (TpPa) materials were synthesized via a solvothermal method. TEM analysis [Figure 1b] confirmed a well-defined core-shell architecture for the synthesized COF@Fe_3O_4 composites. The magnetic Fe_3O_4 core was uniformly encapsulated by a COF shell with an average thickness of approximately 90 nm

[Supplementary Figure 1a], demonstrating the successful coating of COF onto the nanoparticle surfaces. Notably, these intra-shell microporous channels exhibited a highly oriented growth nearly perpendicular to the core surfaces [Supplementary Figures 1b and 1c]. Such a directional alignment underscores the superior long-range order and highly crystalline characteristics of the outer COF layer[33]. As observed from the TEM image [Figure 1c] and SEM image [Supplementary Figure 1d], Pt-SAC/COF@Fe_3O_4 retains an intact spherical morphology and core-shell structure after loading Pt single atoms, with a catalyst particle size of approximately 326 nm. Meanwhile, the HR-TEM image [Figure 1d] reveals no obvious Pt nanoparticles or clusters in the Pt-SAC/COF@Fe_3O_4 catalyst. To further confirm the presence of Pt single atoms, AC HAADF-STEM characterization was performed on Pt-SAC/COF@Fe_3O_4 [Figure 1e]. Isolated bright spots (highlighted by red circles) are distributed on the surface of COF@Fe_3O_4, indicating the successful loading of Pt single atoms with a certain density. To further clarify the elemental distribution within the catalyst, HAADF-STEM [Figure 1f] and corresponding EDS-mapping were conducted on the Pt-SAC/COF@Fe_3O_4 catalyst.

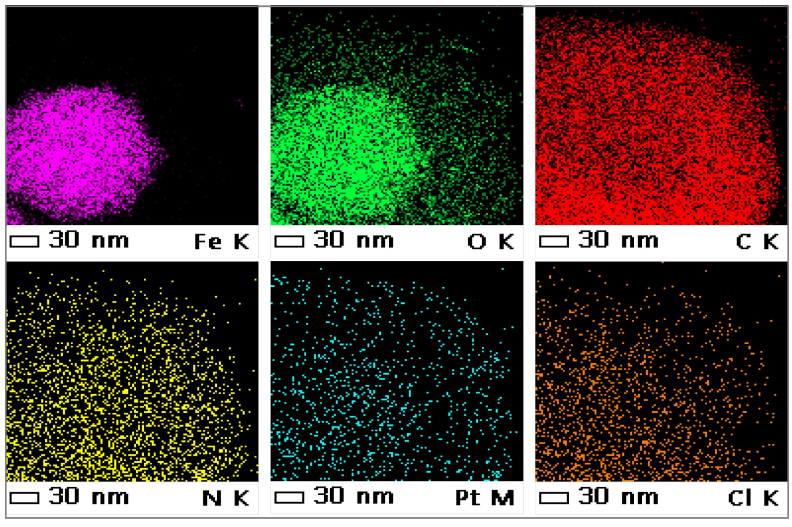

Figure 2. EDS mapping of Fe, O, C, N, Pt and Cl (The scale bar is 30 nm).

The successful synthesis of P-SAC/COF@Fe_3O_4 is evidenced by the widespread distribution of Fe, O, C, N, Pt, and Cl elements over the entire support [Figure 2].

Additionally, the characteristic core-shell framework was confirmed via EDS elemental line scanning [Supplementary Figure 1f], distinguishing a core of Fe/O species surrounded by a predominantly C/N shell.

The core-shell heterostructure of Pt-SAC/COF@Fe_3O_4 was further verified by the XRD analysis [Figure 3a]. In addition, the calcined material did not exhibit discernible peaks corresponding to Pt nanoparticles in XRD analysis. For Pt-SAC/COF@Fe_3O_4, the diffraction peaks observed at 2θ values of 30.28°, 35.46°, 43.40°, 53.28°, 57.14° and 62.76° can be respectively indexed to the (220), (311), (400), (422), (511) and (440) crystallographic planes of Fe_3O_4[34]. The attenuation of Fe_3O_4 diffraction intensities compared to pristine Fe_3O_4 is attributed to the formation of COF shell layer, which induces structural disorder and reduces crystallographic coherence during the encapsulation process.

FTIR spectra [Figure 3b] revealed that the Fe-O bond exhibited a characteristic vibrational absorption peak at 590 cm^{-1}, while a hydroxyl (-OH) absorption peak appeared at 3,422 cm^{-1}, likely attributed to residual moisture in the undried sample. Notably, both Fe-O and -OH absorption peaks showed markedly decreased in COF@Fe_3O_4 and Pt-SAC/COF@Fe_3O_4 composites, demonstrating successful encapsulation of Fe_3O_4 by the COF. Furthermore, the observation of the -NH_2 stretching vibration at 3,338~3,407 cm^{-1} in the Pa precursor, and its subsequent disappearance in both the synthesized COF and the Pt-SAC/COF@Fe_3O_4 composite, confirms the successful formation of the COF structure via covalent bonding. At the same time, distinct bending vibration bands corresponding to the imine linkage (C = N) were observed at ~1,276 cm^{-1} (assigned to C = N in-plane bending), and a stretching vibration peak of the C = N bond in the imine group was detected at ~1,580 cm^{-1}. These spectral features align with the characteristic stretching bands of imine linkages in COFs which confirm the successful preparation of the COF structure. Pt SACs loaded in the surface of COF@Fe_3O_4 to prepare Pt-SAC/COF@Fe_3O_4 through strong

coordination complexation.

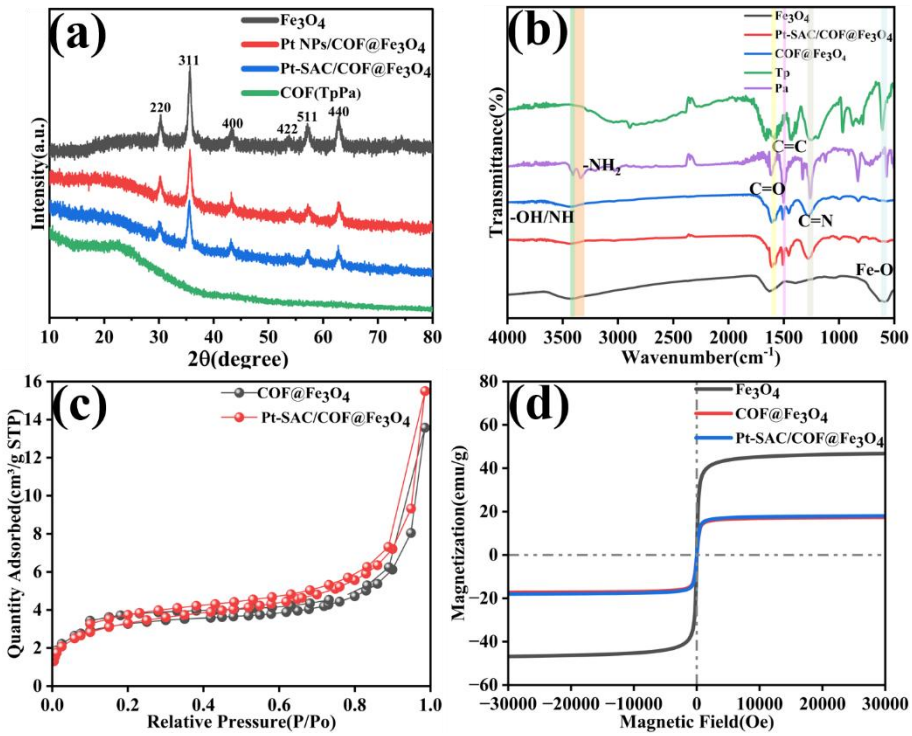

Figure 3. (a) XRD patterns of Fe_3O_4, Pt NPs/COF@Fe_3O_4, Pt-SAC/COF@Fe_3O_4 and COF (TpPa); (b) FTIR spectra of Fe_3O_4, Pt-SAC/COF@Fe_3O_4, COF@Fe_3O_4, Tp and Pa; (c) N_2 sorption/desorption isotherms of COF@Fe_3O_4 and Pt-SAC/COF@Fe_3O_4; (d) Room temperature magnetization curves of Fe_3O_4, COF@Fe_3O_4 and Pt-SAC/COF@Fe_3O_4.

Figure 3c showed the porosities of the prepared COF@Fe_3O_4 and Pt-SAC/COF@Fe_3O_4 by N_2 adsorption-desorption experiment. COF@Fe_3O_4 and Pt-SAC/COF@Fe_3O_4 exhibited type IV reversible isotherms, reflecting a mesoporous structure. Mesoporous materials possessing optimized pore sizes are highly conducive to mass transport and facilitate the exposure of more accessible active sites during catalytic reactions, thereby highlighting the great potential of Pt-SAC/COF@Fe_3O_4.

The magnetic properties of the prepared catalysts were evaluated using a vibrating sample magnetometer (VSM) under an external magnetic field sweeping from -30,000

to +30,000 Oe. The hysteresis loops of Fe_3O_4, COF@Fe_3O_4 and Pt-SAC/COF@Fe_3O_4 were shown in Figure 3d. It can be clearly observed from the graph that COF@Fe_3O_4 and Pt-SAC/COF@Fe_3O_4 exhibited lower saturation magnetization compared with Fe_3O_4 nanoparticles. This might be due to the magnetic shielding effect from COF shell and Pt SACs coated on the surface of Fe_3O_4 nanoparticles. Nonetheless, the magnetization saturation of the catalyst was about 17.98 emu/g and exhibited fast responses within 2 min under the external magnetic field [Supplementary Figure 3], thereby they could easily be separated from solution with a magnet and recycle the catalyst.

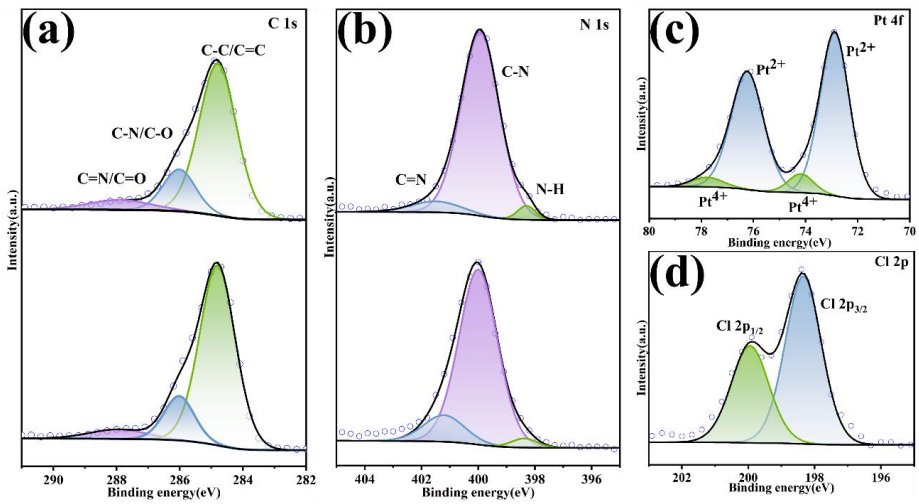

Figure 4. (a-b) XPS spectra of C 1s and N 1s of Pt-SAC/COF@Fe_3O_4 (top) and COF@Fe_3O_4 (bottom); (c-d) XPS spectra of Pt 4f and Cl 2p of Pt-SAC/COF@Fe_3O_4.

The XPS spectra was analyzed to confirm charge transfer and coordination effects within the COF framework and to verify the elemental composition of Pt-SAC/COF@Fe_3O_4. The high-resolution C 1s spectrum [Figure 4a] deconvoluted into three peaks corresponding to C = C/C-C (284.8 eV), C = N (287.9 eV), and C-N/C-O (286.2 eV) consistent with the structure of COF. According to the N 1s spectrum [Figure 4b], two distinct peaks were observed in Pt-SAC/COF@Fe_3O_4 catalyst: one at ~401.4 eV assigned to the -N = C (imine) group and another at ~399.9 eV attributed to N-C in the triazine unit. Notably, the -N = C peak which existed in

Pt-SAC/COF@Fe_3O_4 shifted to a higher binding energy compared to the pristine COF@Fe_3O_4, suggesting electron density reduction at N atoms due to the formation of Pt-N coordination bonds. The high-resolution Pt 4f spectrum [Figure 4c] displayed dual oxidation states: Pt^{4+} ($4f_{7/2}$ at ~74.2 eV and $4f_{5/2}$ at ~77.8 eV) and Pt^{2+} ($4f_{7/2}$ at ~72.9eV and $4f_{5/2}$ at ~76.2 eV). The negative shift in Pt^{4+} binding energy compared to the H_2PtCl_6 precursor indicated that electron transferred from N/O atoms in the COF to Pt^{4+} sites, confirming strong electronic interactions rather than physical adsorption. UV spectrometry also verified the above results, revealing a prominent absorption maximum at 264 nm for the original chloroplatinic acid solution, corresponding to Pt^{4+} [Supplementary Figure 4][35]. After preparation of Pt-SAC/COF@Fe_3O_4, this peak was significantly decreased. Additionally, the Cl 2p spectrum [Figure 4d] displays a characteristic spin-orbit doublet at 199.9 eV and 198.3 eV, assigned to Cl $2p_{1/2}$ and Cl $2p_{3/2}$ of the Pt-Cl species, respectively. This firmly verifies that Cl^- ions are not merely physisorbed on the COF surface, but are chemically coordinated into stable Pt-Cl bonds, thereby anchoring and stabilizing the single-atom Pt sites. The survey spectrum [Supplementary Figure 5] primarily also revealed the presence of C, N, Cl, and Pt while no Fe signal was detected. The absence of Fe was attributed to the complete encapsulation of Fe_3O_4 by the thick COF layer, which exceeded the XPS probing depth (5~10 nm). However, as shown in Supplementary Figure 6, the high-resolution Fe 2p spectrum exhibited characteristic peaks for Fe^{2+} and Fe^{3+}, confirming the existence of Fe_3O_4. Overall, these observations confirm that the preparation of Pt-SAC/COF@Fe_3O_4 was successful.

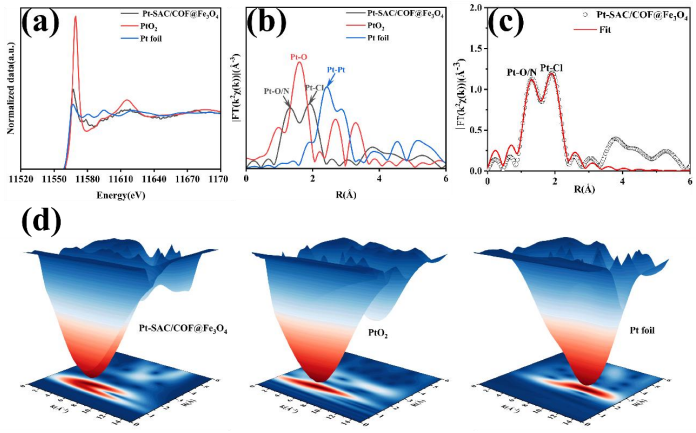

Figure 5. (a) Pt L_3-edge XANES spectra of Pt-SAC/COF@Fe_3O_4 and reference samples; (b) FT-EXAFS analysis of Pt-SAC/COF@Fe_3O_4 and reference samples at the Pt L_3-edge resulting in R spaces; (c) The results of R space FT k^2 weighted $\chi(k)$ function fitting curves of the Pt L_3-edge EXAFS; (d) Pt L_3-edge EXAFS of Pt-SAC/COF@Fe_3O_4, PtO_2 and Pt foil.

XAFS was employed to investigate the chemical states and coordination environment of Pt atoms in the as-prepared Pt-SAC/COF@Fe_3O_4 catalyst. As estimated from the Pt L_3-edge XANES (X-ray absorption near-edge structure) spectra of Pt-SAC/COF@Fe_3O_4 [Figure 5a], the absorption edge position of Pt in Pt-SAC/COF@Fe_3O_4 was located between those of Pt foil and PtO_2, indicating that the valence state of Pt is between 0 and +4[36], which is consistent with the high-resolution Pt 4f spectral data [Figure 4c]. Subsequently, the FT-EXAFS (fourier transform extended X-ray absorption fine structure) spectra in R-space were used to further analyze the local coordination environment of the central Pt atoms, and the obtained data were compared with those of the reference samples (Pt foil and PtO_2). As shown in Figure 5b, the main peak at ~1.25 Å is assigned to the Pt-O/N scattering path, and the prominent peak at ~1.8 Å corresponds to the Pt-Cl scattering path. No peaks corresponding to Pt foil (~2.58 Å) or PtO_2 (~1.63 Å) are observed, demonstrating the isolated state of Pt single atoms, which is in good agreement with the AC HAADF-STEM results[37,38]. Meanwhile, the EXAFS (extended X-ray absorption fine structure) fitting curves [Figure 5c] and coordination parameters [Supplementary Table

1] demonstrated that the local coordination environment of the central Pt atom consists of one N atom, one O atom, and two Cl atoms, confirming the coordination structure of the Pt-SAC/COF@Fe_3O_4 single-atom catalyst as N/O-Pt-Cl_2.

To accurately identify the distinct backscattering atoms, wavelet transform (WT) analysis was performed on the Pt L_3-edge EXAFS spectra of Pt-SAC/COF@Fe_3O_4. As shown in Figure 5d, the WT contour of Pt-SAC/COF@Fe3O4 exhibits the maximum intensity at approximately 5.5 Å, which is fully consistent with the characteristic feature of the N/O-Pt-Cl_2 coordination. This signal is distinctly different from those of Pt foil (Pt-Pt coordination) and PtO_2 (Pt-O coordination), thus providing convincing evidence for the existence of the N/O-Pt-Cl_2 coordination structure[39].

Optimization of the reaction conditions of the anti-markovnikov alkene hydrosilylation

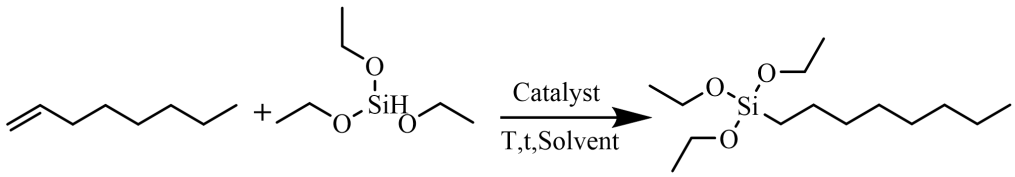

Scheme 2. Pt-SAC/COF@Fe_3O_4 catalyzes the anti-Markovnikov hydrosilylation of alkenes.

The catalytic performance of Pt-SAC/COF@Fe_3O_4 was validated by investigating the experimental conditions for the anti-Markovnikov hydrosilylation of 1-octene with triethoxysilane. As shown in Table 1, the product yield and selectivity reached their maxima of 93% and 98%, respectively, at 10 h when the reaction time was prolonged from 8 h to 10 h [Table 1, entries 1-3]. The catalytic yield decreased when the reaction time was either shortened or extended. This can be rationalized by the regular pore structure of the COF support, which requires sufficient time for substrates to access and interact with Pt single-atom sites. At short reaction times, the adsorption, activation,

and conversion of substrates on the catalyst surface are incomplete, leading to low conversion. At excessively long times, side reactions may occur or strong adsorption of products on active sites can induce site poisoning, further reducing catalytic efficiency.

Table 1. Exploration of conditions for Pt-SAC/COF@Fe_3O_4 catalytic anti-Markovnikov reaction of octene with triethoxysilane.

Entry	Catalyst	$n_{(silane)}/n_{(olefin)}$	Catal. (wt.%)	T.(°C)	Time (h)	Solvent	Yield	Sel.
1	Pt-SAC/COF@Fe_3O_4	1.7	0.75	80	8	p-xylen	72	97
2	Pt-SAC/COF@Fe_3O_4	1.7	0.75	80	10	p-xylen	93	98
3	Pt-SAC/COF@Fe_3O_4	1.7	0.75	80	12	p-xylen	68	97
4	Pt-SAC/COF@Fe_3O_4	1.7	0.75	60	10	p-xylen	72	99
5	Pt-SAC/COF@Fe_3O_4	1.7	0.75	100	10	p-xylen	28	96
6	Pt-SAC/COF@Fe_3O_4	1.7	0.75	80	10	THF	5	42
7	Pt-SAC/COF@Fe_3O_4	1.7	0.75	80	10	EA	40	50
8	Pt-SAC/COF@Fe_3O_4	1.7	0.75	80	10	ACN	16	80
9	Pt-SAC/COF@Fe_3O_4	1.7	0.75	80	10	toluene	85	70
10	Pt-SAC/COF@Fe_3O_4	1.5	0.75	80	10	p-xylen	68	99
11	Pt-SAC/COF@Fe_3O_4	2	0.75	80	10	p-xylen	87	93
12	Pt-SAC/COF@Fe_3O_4	1	0.75	80	10	p-xylen	56	99
13	Pt-SAC/COF@Fe_3O_4	1.7	0.38	80	10	p-xylen	78	99
14	Pt-SAC/COF@Fe_3O_4	1.7	1.5	80	10	p-xylen	63	99
15	Fe_3O_4[a]	1.7	-	80	10	p-xylen	-	-
16	COF@Fe_3O_4[a]	1.7	-	80	10	p-xylen	-	-
17	Pt	1.7	0.75	80	10	p-xylen	59	98

18	H_2PtCl_6[b]	1.7	0.75	80	10	p-xylen	53	95

[a] Reaction condition: triethoxysilane (1.7 mmol), 1-octene (1 mmol), catalyst (10 mg), p-xylene (2 mL), at 80 °C for 10 h. [b] Reaction condition: triethoxysilane (1.7 mmol), 1-octene (1 mmol), catalyst [100 μL, 10 mg/mL, in acetonitrile (2 mL)], p-xylene (2 mL), at 80 °C for 10 h.

Furthermore, the reaction temperature was screened under the optimized reaction time and catalyst dosage [Table 1, entries 4-5]. The highest catalytic efficiency was achieved at 80°C, whereas a mere 20 °C decrease led to a sharp drop in yield to 72%, demonstrating that temperature exerts a significant influence on catalytic performance. In addition, different solvents and substrate molar ratios were investigated to compare product yield and selectivity, both of which were markedly affected by these parameters [Table 1, entries 6-12]. The optimal molar ratio of silane to alkene was 1.7, with p-xylene as the preferred solvent. In the anti-Markovnikov hydrosilylation of alkenes, the highest yield (93%) was obtained with 10 mg of Pt-SAC/COF@Fe_3O_4 (Pt content 0.75 wt.%). At 5 mg, insufficient Pt single-atom active sites resulted in incomplete conversion. At 15 mg, increased mass-transfer resistance, shielding of active sites, and enhanced side reactions caused a notable decrease in yield (Table 1, entries 13-14). These results indicate that the catalyst enables high product yield at a low noble-metal loading, reflecting its outstanding catalytic activity. An appropriate catalyst dosage achieves the optimal balance between the number of active sites and substrate mass transfer, ensuring the efficient operation of the Chalk-Harrod pathway and maintaining high anti-Markovnikov selectivity. To verify whether Pt single atoms serve as the catalytically active centers, Fe_3O_4, COF@Fe_3O_4, Pt NPs/COF@Fe_3O_4, and H_2PtCl_6 were used as control samples. No reaction occurred over Fe_3O_4 and COF@Fe_3O_4 within 10 h, indicating that the supports are not catalytically active [Table 1, entries 15-16]. The inactivity of magnetic Fe_3O_4 arises mainly from its inappropriate electronic structure and coordination environment, which are unable to effectively activate the Si-H bond or stabilize reaction intermediates. In contrast, Pt NPs/COF@Fe_3O_4 and H_2PtCl_6 exhibited moderate catalytic activity, confirming that

Pt^{4+} can also act as active sites. Nevertheless, their catalytic performance was far inferior to that of Pt-SAC/COF@Fe_3O_4 [Table 1, entries 17-18].

Exploration of application potential and experimental study on stability performance of catalysts

To investigate the substrate generality of Pt-SAC/COF@Fe_3O_4 under the optimized reaction conditions, the reactions of various alkenes with different silanes were examined. As shown in Supplementary Table 2, linear alkenes containing terminal C = C bonds could be smoothly converted into the desired anti-Markovnikov products with favorable yields and selectivities. As listed in Supplementary Table 2 (entry 1), 1-dodecene and triethoxysilane were successfully transformed into the target anti-Markovnikov product with a yield of 97% and a selectivity of 88%. In addition, different types of silanes (e.g., $HSiEt_3$) also reacted well with 1-octene, affording the corresponding product with 95% yield and 99% selectivity (Supplementary Table 2, entry 2). When 1-dodecene and triethylsilane were used as reactants, the target product was obtained with 73% yield and 99% selectivity (entry 3). The anti-Markovnikov hydrosilylation of 1-undecene with triethylsilane catalyzed by Pt-SAC/COF@Fe_3O_4 at 80°C gave the corresponding product with 73% yield and 99% selectivity (entry 4). In short, the broad substrate scope demonstrates the promising application potential of the Pt-SAC/COF@Fe_3O_4 catalyst. The superior catalytic performance of Pt-SAC/COF@Fe_3O_4 is mainly attributed to the abundant catalytically active sites on the surface of the COF support and the efficient utilization of atomically dispersed Pt. Moreover, the strong coordination interactions between Pt single atoms and N, O, Cl heteroatoms further enhance the adsorption of alkenes at the active sites, resulting in robust coordination bonding between the metal centers and the support. In contrast, traditional homogeneous catalysts such as Speier's and Karstedt's systems often suffer from decomposition and induce undesired side reactions, which significantly deteriorate product quality. Furthermore, as displayed in Figure 6a, commercial Pt/C catalyst exhibited markedly lower yield (62%) and selectivity (81%) toward

n-octyltriethoxysilane. All these results confirm that Pt-SAC/COF@Fe_3O_4 is a highly promising catalyst for the anti-Markovnikov hydrosilylation of alkene.

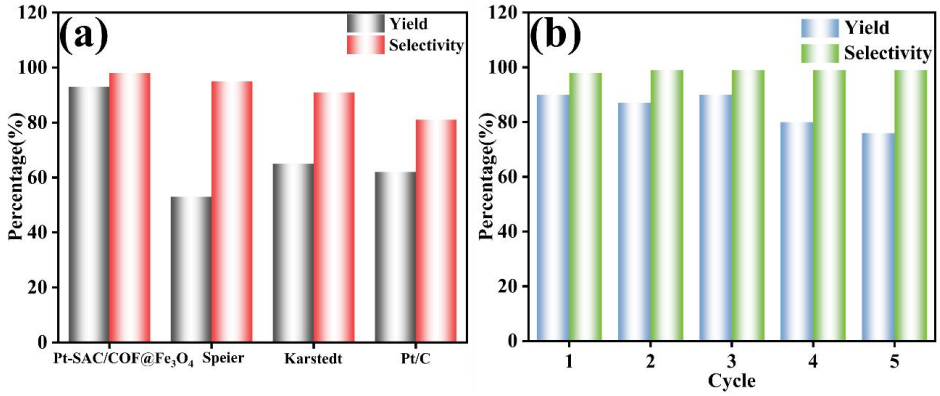

Figure 6. (a) Comparison of the yield and selectivity with other commercial catalysts; (b) The recyclability of Pt-SAC/COF@Fe_3O_4 catalyst.

The recovery and reusability of Pt-SAC/COF@Fe_3O_4 were examined by hydrosilylation between 1-octene and triethoxysilane under optimal reaction conditions. The catalysts were collected by centrifugation and washed with deionized aqueous and ethanol for the next cycle. As shown in Figure 6b, with most yield of 1-octene, the selectivity of the anti-Markovnikov product was unchanged during 5 reaction cycles, indicative of the excellent recycling stability of the catalysts. The ICP-OES results (0.53 wt.%) of the recycled catalysts obtained after 5 cycles revealed slight but negligible loss of Pt. The crystal structure remained intact after recycling, as evidenced by the unaltered XRD patterns [Supplementary Figure 10], underscoring the exceptional stability of the catalyst. These findings collectively manifest that the atomically dispersed single sites endow Pt-SAC/COF@Fe_3O_4 with superior catalytic activity and robust reusability for alkene hydrosilylation. Pt-SAC/COF@Fe_3O_4 demonstrated enhanced recyclability through the magnetic properties imparted by the Fe_3O_4 component, enabling efficient catalyst recovery via external magnetic fields. This hybrid system exhibits superior reusability while maintaining catalytic performance over multiple cycles. Significantly, the atomic dispersion of Pt species maximizes metal utilization efficiency and substantially mitigates noble metal leaching.

These combined attributed including magnetic separation capability, exceptional structural stability and minimized platinum loss-present a promising strategy for developing economically viable and sustainable catalytic systems for industrial-scale silane production.

CONCLUSION

In summary, we have constructed a magnetic porous COF carrier, which serves as an ideal support for anchoring and stabilizing Pt single atoms. The successful synthesis of the Pt-SAC/COF@Fe_3O_4 catalyst with a Pt loading of 0.75 wt.% under mild conditions (125 ^oC) was confirmed by AC HAADF-STEM and XAS characterization, demonstrating remarkable catalytic activity and stability in the anti-Markovnikov hydrosilylation of alkenes compared to other commercially Pt catalysts. The characterization results verified that the Pt single atoms are anchored to form a four-coordinated configuration with one N atom, one O atom, and two Cl atoms. Comparative studies with pristine COF@Fe_3O_4 carriers and Fe_3O_4 nanoparticles revealed that the superior catalytic performance originates predominantly from the atomically dispersed Pt active centers. The introduction of Fe_3O_4 nanoparticles endows the catalyst with highly efficient magnetic recyclability, enabling rapid separation within only 2 min, which effectively addresses the challenge of catalyst separation. This results clearly highlight the promising potential of magnetic COF-based Pt single-atom catalysts for hydrosilylation applications and provides a strategic pathway for designing industrially viable noble metal catalysts with integrated magnetic functionality.

DECLARATIONS

Authors' contributions

Conceptualization: LY.S;

Investigation: QH.D;

Methodology: YQ.S, GD.C;

Supervision: YQ.S, XW.Z;

Writing-review & editing: ZF.H, ZC.D, ZB.G;

Funding acquisition: ZB.G, YQ.S, XW.Z;

All authors have read and agreed to the published version of the manuscript.

Availability of data and materials

All data needed to support the conclusions in the paper are presented in the manuscript and/or the Electronic Supplementary Material. Additional data related to this paper may be requested from the corresponding author upon request.

AI and AI-assisted Tools Statement

During the preparation of this manuscript, the AI tool ChatGPT (version 5.4, released 2026-03-05) was used solely for language polishing. The tool did not influence the study design, data collection, analysis, interpretation, or the scientific content of the work. All authors take full responsibility for the accuracy, integrity, and final content of the manuscript.

Financial support and sponsorship

This work was supported by the National Natural Science Foundation of China (No. 22075122 and 22371108), Natural Science Foundation of Shandong Province (No. ZR2020QB170 and ZR2024MB125), Taishan Scholar Foundation of Shandong Province (tsqn202211242).

Conflicts of interest

All authors declared that there are no conflicts of interest.

Ethical approval and consent to participate

Not applicable.

Consent for publication

Not applicable.

REFERENCES

1. Singh M, Teodorescu DL, Rowlett M, et al., A tunable soft silicone bioadhesive for secure anchoring of diverse medical devices to wet biological tissue. *Adv. Mater*. **2024**, *36*, 2307288.[DOI:10.1002/adma.202307288]

2. Wang H, Zhang X, Li Y, Xu L. Siloxane-based organosilicon materials in electrochemical energy storage devices. *Angew. Chem. Int. Ed*. **2022**, *61*, e202210851.[DOI:10.1002/anie.202210851]

3. Wu J, Zhu Q, Liu S, et al., Electrochemically driven enzymatic oxidative desymmetrization for the enantioselective construction of silicon stereocenter. *Angew. Chem. Int. Ed*. **2026**, *65*, e3445735.[DOI:10.1002/anie.3445735]

4. Chatterjee A, Sen S, Ramakanth D, Singh S, Maji PK. Unravelling polysilazanes: Synthesis, structure-property insights and versatile coating applications. *Adv. in Colloid and Interface Sci*. **2025**, *342*, 103508.[DOI:10.1016/j.cis.2025.103508]

5. Xiao H, Zhang K, Gui T, Zhou S. Facile fabrication of polyacrylate-siloxane antifouling coatings with self-generated biomimetic surface. *Chem. Eng. J*. **2025**, *516*, 164087.[DOI:10.2139/ssrn.5177166]

6. Speier JL, Webster JA, Barnes GH. The addition of silicon hydrides to olefinic double bonds. Part II. The use of group VIII metal catalysts. *J. Am. Chem. Soc*. **1957**, *79*, 974-9.[DOI:10.1021/ja01561a054]

7. Li Z, Millward AR, Biswas S, et al., Enone as a process aid for the highly efficient synthesis of Karstedt's catalyst: Probing the mechanism of dissolution of platinum(II) chloride. *ACS Catal*. **2023**, *13*, 12494-505.[DOI:10.1021/acscatal.3c02226]

8. Lu M, Kang X, Qian C, et al., Modeled single-atomic-site Pt catalyst with well-defined coordination structure for hydrosilylation reaction. *Angew. Chem. Int. Ed*. **2025**, *64*, e202508064.[DOI:10.1002/anie.202508064]

9. Tereshchenko AA, Goncharova IK, Zagrebaev AD, et al., Heterophase

Pt/EG-catalyzed hydrosilylation in droplet microfluidics: Spectral monitoring and efficient 3D-printed reactors. *Chem. Eng. J.* **2024**, *498*, 155016.[DOI:10.1016/j.cej.2024.155016]

10. Li LJ, He P, Zhang XY, Zhu SF. Iron-catalyzed anti-Markovnikov allylzincation of terminal alkynes. *J. Am. Chem. Soc*. **2026**, *148*, 9698-708.[DOI:10.1021/jacs.5c21100]

11. Pan G, Hu C, Hong S, et al., Biomimetic caged platinum catalyst for hydrosilylation reaction with high site selectivity. *Nat. Commun*. **2021**, *12*, 64.[DOI:10.1038/s41467-020-20233-w]

12. Long X, Zhu D, Zhu S. Cobalt-catalyzed chemoselective and divergent synthesis of vinylsilanes through hydrosilylation of acetylene. *ACS Catal*. **2025**, *15*, 4429-40.[DOI:10.1021/acscatal.5c00006]

13. Bai D, Zhong K, Chang L, et al., Nickel-catalyzed regiodivergent hydrosilylation of α-(fluoroalkyl)styrenes without defluorination. *Nat. Commun*. **2024**, *15*, 6360.[DOI:10.1038/s41467-024-50743-w]

14. Li P, Lyu J, Zhao Y, et al., Towards highly efficient selective hydrogenation: The role of single-atom catalysts. *Chin. J. Catal*. **2026**, *81*, 69-96.[DOI:10.1016/S1872-2067(25)64906-0]

15. Li YT, Cui WG, Huo YF, et al., Acetylene semi-hydrogenation catalyzed by Pd single atoms sandwiched in zeolitic imidazolate frameworks *via* hydrogen activation and spillover. *Mater. Horiz*. **2025**, *12*, 2351-9.[DOI:10.1039/D4MH01787K]

16. Chen W, Ma B, Zou R. Rational design and controlled synthesis of MOF-derived single-atom catalysts. *Acc. Mater. Res*. **2025**, **6**, 210-20.[DOI:10.1021/accountsmr.4c00330]

17. Chen M, Fan Y, Wu S, et al., Co-implanting the single-atom Pd sites and triphenylphosphine promoters into COFs materials for highly efficient selective hydrogenation of acetylene. *Chem. En. J.* **2025**, *515*, 163744.[DOI:10.1016/j.cej.2025.163744]

18. Tang W, Zeng J, Bian F, Lin H, Zhao H, Lv Z. Engineering heteroatomic structures in Pt single-atom anchored covalent organic frameworks for enhanced photocatalytic

hydrogen evolution reaction. *J. Mater. Chem*. **2025**, *25*, 19682-94.[DOI:10.2139/ssrn.5118948]

19. Han X, Duan P, Xu Y, et al., Aprotic solvent-mediated microenvironment engineering for single-atom catalysts enables selective nitroarene hydrogenation. *Adv. Funct. Mater*. **2026**, e75375.[DOI:10.1002/adfm.75375]

20. Gao C, Lyu F, Yin Y. Encapsulated metal nanoparticles for catalysis. *Chem. Rev*. **2021**, *121*, 834-81.[DOI:10.1021/acs.chemrev.0c00237]

21. Yusran Y, Li H, Guan X, Fang Q, Qiu S. Covalent organic frameworks for catalysis. *J. Energy Chem*. **2020**, *2*, 100035.[DOI:10.1016/j.enchem.2020.100035]

22. Ou L, Xue Z, Li B, et al., Nitrogen-containing linkage-bonds in covalent organic frameworks: Synthesis and applications. *Chin. Chem.l Lett*. **2025**, *36*, 110294.[DOI:10.1016/j.cclet.2024.110294]

23. Deng Y, Zhang Z, Du P, et al., Embedding ultrasmall Au clusters into the pores of a covalent organic framework for enhanced photostability and photocatalytic performance. *Angew. Chem. Int. Ed*. **2020**, *59*, 6082-9.[DOI:10.1002/anie.201916154]

24. Qian Y, Jiang HL. Structural regulation of covalent organic frameworks for catalysis. *Acc. Chem. Res*. **2024**, *57*, 1214-26.[DOI:10.1021/acs.accounts.4c00061]

25. Niu L, Zhao X, Tang Z, et al., One-step mechanochemical preparation of magnetic covalent organic framework for the degradation of organic pollutants by heterogeneous and homogeneous Fenton-like synergistic reaction. *Sep. Purif. Technol*. **2022**, *294*, 121145.[DOI:10.1016/j.seppur.2022.121145]

26. Ke F, Yuan J, Zhang C, Ye S, Ramachandraiah K, Pang H. Core-shell nanostructured metal-organic frameworks with encapsulated magnetic nanoparticles for magnetically recyclable catalysis. *Coord. Chem. Rev*. **2024**, *518*, 216116.[DOI:10.1016/j.ccr.2024.216116]

27. Uthappa UT, Niu JC, Zhou Y, Wang B. Fuel-free magnetic COF-alginate microbead motors for active removal of dual carcinogenic pollutants. *Chem. Eng. J*. **2025**, *526*, 170912.[DOI:10.1016/j.cej.2025.170912]

28. Azizi N, Heidarzadeh F, Farzaneh F. Facile fabrication of porous magnetic covalent

organic frameworks as robust platform for multicomponent reaction. *Appl. Organom Chem*. **2021**, *35*, e6373.[DOI:10.1002/aoc.6373]

29. Mishra K, Datta Khanal H, Rok Lee Y. Facile *N* -Formylation of Amines on Magnetic Fe_3O_4-CuO Nanocomposites. *Eur. J. Org. Chem*. **2021**, *2021*, 4477-84.[DOI:10.1002/ejoc.202100872]

30. Patra D, Panja S, Saha A. C-C cross-coupling reactions of organosilanes with terminal alkenes and allylic acetates asing PdII catalyst supported on starch coated magnetic nanoparticles. *Eur. J. Org. Chem*. **2020**, *2020*, 878-83.[DOI:10.1002/ejoc.201901812]

31. Chen R, Chen X, Zhou Y, et al., "Three-in-One" multifunctional nanohybrids with colorimetric magnetic catalytic activities to enhance immunochromatographic diagnosis. *ACS Nano*. **2022**, *16*, 3351-61.[DOI:10.1021/acsnano.2c00008]

32. Sun T, Zhang H, Wang Y, et al., Covalent organic frameworks anchoring single-atom Pt for three-phase interface-assisted photocatalytic overall water splitting. *Angew. Chem. Int. Ed*. **2025**, *64*, e202515397.[DOI:10.1002/anie.202515397]

33. Liang D, Zhang X, Wang Y, et al., Magnetic covalent organic framework nanospheres-based miRNA biosensor for sensitive glioma detection. *Bioact. Mater*. **2022**, *14*, 145-51.[DOI:10.1016/j.bioactmat.2021.11.033]

34. Zhang Y, Zhang J, Tian M, Chu G, Quan C. Fabrication of amino-functionalized Fe_3O_4@$Cu_3(BTC)_2$ for heterogeneous Knoevenagel condensation. *Chin. J. Catal*. **2016**, *37*, 420-7.[DOI:10.1016/S1872-2067(15)61013-0]

35. Bai Y, Zhang S, Deng Y, et al., Use of functionalized PEG with 4-aminobenzoic acid stabilized platinum nanoparticles as an efficient catalyst for the hydrosilylation of alkenes. *J. Colloid and Interface Sci*. **2013**, *394*, 428-33.[DOI:10.1016/j.jcis.2012.11.048]

36. Dong P, Wang Y, Zhang A, Cheng T, Xi X, Zhang J. Platinum single atoms anchored on a covalent organic framework: Boosting active sites for photocatalytic hydrogen evolution. *ACS Catal*. **2021**, *11*, 13266-79.[DOI:10.1021/acscatal.1c03441]

37. Zhao C, Xu S, Qin W, et al., Elucidating metal coordination interactions in

Pt-impregnated β-ketoenamine-imine covalent organic frameworks for efficient photocatalytic hydrogen production. *Adv. Funct. Mater*. **2026**, *36*, e74589.[DOI:10.1002/adfm.74589]

38. Wang Q, Ling W, Lu Y, et al., Synergistic stabilization of Pt single atoms by Cl and Ru for industrial-scale current density hydrogen production. *Angew. Chem. Int. Ed*. **2025**, *64*, e202506619.[DOI:10.1002/anie.202506619]

39. Wu H, Li D, Zhao B, et al., Magnetic covalent organic framework nanocomposites as a new adsorbent for the determination of polycyclic aromatic hydrocarbons in water and food samples. *Anal. Methods*. **2021**, *13*, 2847-56.[DOI:10.1039/D1AY00496D]